Inorganic Chemistry

Article

pubs.acs.org/IC

Mn_3 Single-Molecule Magnets and Mn_6/Mn_9 Clusters from the Use of Methyl 2-Pyridyl Ketone Oxime in Manganese Phosphinate and Phosphonate Chemistry

Olajuyigbe A. Adebayo,[†] Khalil A. Abboud, and George Christou*

Department of Chemistry, University of Florida, Gainesville, Florida 32611-7200, United States

Supporting Information

ABSTRACT: The syntheses, structures, and magnetochemical properties are reported for five new Mn clusters: $[Mn^{III}_3O(O_2PPh_2)_3(mpko)_3](ClO_4)$ (**1**), $[Mn^{III}_3O(O_2PPh_2)_3(ppko)_3](ClO_4)$ (**2**) $[Mn^{III}_6O_2(OMe)_4(O_2PPh_2)_4(mpko)_4](ClO_4)_2$ (**3**), $[Mn^{III}_8Mn^{II}O_6(O_2CMe)_7(O_3PPh)_2(mpko)_3(H_2O)]$ (**4**), and $[Mn^{III}_2Mn^{II}O(mpko)_3(H_2O)_4(ClO_4)_2](ClO_4)$ (**5**), where $mpko^-$ (or $ppko^-$) is the anion of methyl (or phenyl) 2-pyridyl ketone oxime. **1** was obtained by carboxylate substitution on $[Mn^{III}_3O(O_2CMe)_3(mpko)_3](ClO_4)$ by treatment with diphenylphosphinic acid (Ph_2PO_2H). The comproportionation reaction between $Mn(ClO_4)_2$ and $NBu^n_4MnO_4$ in the presence of Ph_2PO_2H and ppkoH in EtOH, or mpkoH in MeOH, led to **2** and **3**, respectively. **4** was obtained as was **3**, but with phenylphosphonic acid ($PhPO_3H_2$) instead of Ph_2PO_2H. **5** was obtained by aerial oxidation of $Mn(ClO_4)_2$ in the presence of mpkoH. **1** and **2** contain a triangular Mn_3 core, **3** comprises the fusion of two Mn_3 units of **1** by MeO^- bridges, and **4** has a cagelike structure. **5** is similar to **1** in possessing a triangular core. Variable-temperature, solid-state direct-current (dc) and alternating-current (ac) magnetic data were collected on **1**−**5**: **1** and **2** exhibit ferromagnetic Mn···Mn exchange interactions, $S = 6$ ground states, and are new single-molecule magnets (SMMs). **3**−**5** possess $S = 4$, $^5/_2$, and $^5/_2$ ground states, respectively, from dominant antiferromagnetic interactions. Fits of dc magnetization data in the 1.8−10.0 K and 10−70 kG ranges gave D and g values of: −0.29(2) cm^{-1} and 1.94(1) for **1**, −0.38(2) cm^{-1} and 1.99(1) for **2**, −0.29(2) cm^{-1} and 1.96(1) for **3**, −1.26(4) cm^{-1} and 1.99(2) for **4**, −1.41(4) cm^{-1} and 1.98(2) for **5**, where D is the axial zero-field splitting parameter.

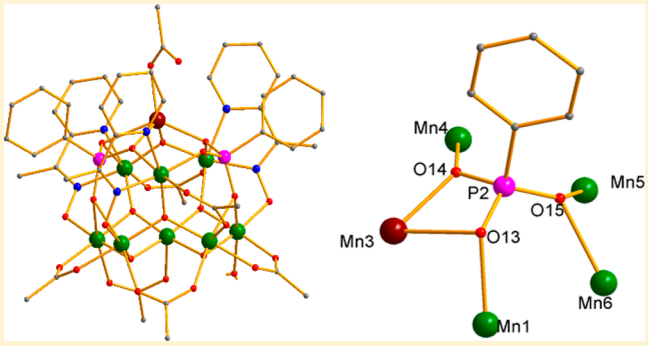

INTRODUCTION

Manganese-oxo cluster chemistry holds a special place in the field of molecular magnetism and single-molecule magnets (SMMs). The latter are molecular superparamagnets below a blocking temperature, T_B, due to a combination of large ground-state magnetic moment and Ising-type magnetoanisotropy that results in a significant energy barrier (vs kT) to reversal of the magnetization vector.[1,2] Mn chemistry was the area in which the latter new magnetic phenomenon was discovered, and the subsequent flood of new (mainly) Mn_x clusters that were reported over the subsequent decade or so led to a great "inflation" of the field and its establishment as a deep-rooted new area of inorganic chemistry and molecular nanomaterials.[3,4] Its subsequent expansion into other d and/or f metal chemistry has led to a dizzying array of high-nuclearity compounds, new structural types, magnetic behaviors, and theoretical understanding.[5−11] The very recent report of an SMM operating at 60 K is the true icing on the cake of the first quarter-century of this field,[12] and it presages an exciting age of next-generation science from this area.

One of the spin-offs from the SMM area has been the development of many fascinating synthetic procedures to metal-oxo clusters with a variety of ligand types, as well as procedures for their modification. Coupled with the general advantages of molecular chemistry, namely, monodispersity, solubility, and crystallinity, this has also led to discovery of new quantum physics for nanomagnetism, such as quantum tunneling of the magnetization vector (QTM),[13] quantum phase interference,[14] exchange-biased QTM,[15,16] and others of relevance to new technologies.[17,18]

Developing methods for the synthesis and modification of coordination-cluster SMMs has been one of our group's interests, including from comproportionation,[19] reductive aggregation,[20] alcoholysis,[21] and others. The work described herein is relevant to previous investigations of the effect of substituting the carboxylate ligands in $Mn/O/RCO_2^-$ clusters with "pseudocarboxylates" (i.e., having an XO_2^- unit that can bridge like a carboxylate, e.g., in the common $\eta^1{:}\eta^1{:}\mu$ mode),

Received: July 13, 2017
Published: August 30, 2017

DOI: 10.1021/acs.inorgchem.7b01793
Inorg. Chem. 2017, 56, 11352−11364

either pre- or postsynthetically. A main objective is to assess the effect of the different electronic (e.g., pK_a) and/or steric properties of the pseudocarboxylate or as a means to facilitate some desired objective such as deposition of an SMM on a surface.[22] Pseudocarboxylates that have been used span various types, namely, with X = N, P, As, S, and Se. In fact, we and others have had little success in replacing all the carboxylates without changing the core structure or nuclearity, except when the number of carboxylates is small compared to the nuclearity of the cluster.[23] For example, partial substitution of $[Mn_{12}O_{12}(O_2CR)_{16}(H_2O)_4]$[4,24] SMMs can be accomplished to give $[Mn_{12}O_{12}(O_2CR)_{16-x}(L)_x(H_2O)_y]$ by reactions with HNO_3 ($x = 4$, $y = 4$), diphenylphosphinic acid (Ph_2PO_2H) ($x = 8$ or 9, $y = 4$),[25] diphenylphosphoric acid ($(PhO)_2PO_2H$) ($x = 4$, $y = 0$),[26] or benzenesulfonic acid ($PhSO_3H$) ($x = 8$, $y = 4$),[27] but attempts to force all carboxylates to be substituted by these ligands,[27] or the use of benzeneseleninic acid ($PhSeO_2H$)[28] or dimethylarsenic acid (Me_2AsO_2H),[29] causes rupture of the Mn_{12} core and a different nuclearity product. This has thus made difficult comparisons of carboxylate SMMs with their pseudocarboxylate analogues.

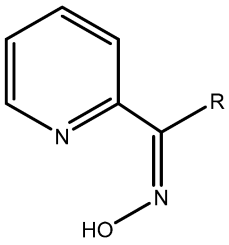

R = Me (mpkoH) or Ph (ppkoH)

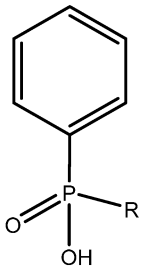

R = Ph (Ph_2PO_2H) = OH ($PhPO_3H_2$)

We have recently been working with the $[Mn_3O(O_2CR)_3(mpko)_3](ClO_4)$ (mpkoH = methyl(2-pyridyl)ketone oxime) SMM family with $S = 6$ ground states[16b,30] discovered by the Perlepes group.[31] We decided to investigate its carboxylate-substitution reactions with Ph_2PO_2H as well as with phenylphosphonic acid ($PhPO_3H_2$) for comparison. As a further comparison, we also investigated the products obtained from the reactions between these P-based reagents and other Mn sources, including simple Mn^{II} salts. We herein report the results of this study, which include the first examples of Mn_3/mpko chemistry with such ligands, and the structural and magnetic properties of the obtained products.

EXPERIMENTAL SECTION

Synthesis. All preparations were performed under aerobic conditions using chemicals and solvents as received. $N^nBu_4MnO_4$,[32] mpkoH,[33] ppkoH,[34] and $[Mn_3O(O_2CMe)_6(py)_3](ClO_4)$[35] were prepared as described elsewhere. ppkoH = phenyl(2-pyridyl)ketone oxime. ***Caution!*** *Although no such behavior was observed, perchlorate salts and $N^nBu_4MnO_4$ are potentially explosive and should always be used in small quantities and with extreme care.*

$[Mn_3O(O_2PPh_2)_3(mpko)_3](ClO_4)$ (1). *Method A.* Ph_2PO_2H (0.60 mmol, 0.13 g) was added to a stirred solution of $[Mn_3O(O_2CMe)_3(mpko)_3](ClO_4)$ (0.20 mmol, 0.17 g) in CH_2Cl_2/MeCN (20 mL, 1:2 v/v). The resulting dark brown solution was stirred for 3 h, and then the solvent was removed under vacuum using a rotary evaporator. In a step repeated twice, toluene (20 mL) was added, the mixture was stirred for 15 min, and the solvent was removed under vacuum. The resulting black residue was dissolved in CH_2Cl_2 (25 mL) and filtered, and the filtrate was layered with hexane (25 mL). Dark brown X-ray quality crystals of $\mathbf{1}\cdot 5CH_2Cl_2$ formed within 5 d, and they were collected by filtration, washed copiously with CH_2Cl_2 and hexane, and dried under vacuum. The yield was 88% based on Mn. Calcd (Found) for $\mathbf{1}\cdot H_2O$ ($C_{57}H_{53}ClN_6O_{15}P_3Mn_3$): C, 50.52 (50.15); H, 3.94 (3.53); N, 6.20 (5.87)%. Selected IR data (KBr, cm^{-1}): 3441(br), 3054(w), 2068(w), 1601(s), 1521 (s), 1476(s), 1437(s), 1384(s), 1264(m), 1190(m), 1119(m), 1034(m), 1010(m), 992(m), 728(s0, 697(s), 657(m), 622(s), 555(m), 529(m), 470(m), 419(w).

Method B. Solid mpkoH (0.60 mmol, 0.08 g) was added to a stirred brown solution of $[Mn_3O(O_2CMe)_6(py)_3](ClO_4)$ (0.2 mmol, 0.18 g) in MeOH/MeCN (15 mL, 1:2 v/v), and the resulting dark brown solution was stirred for a further 30 min. Ph_2PO_2H (0.60 mmol, 0.13 g) dissolved in CH_2Cl_2 (5 mL) was added to the solution and stirred for a further 4 h. The solvents were then removed using a rotary evaporator. In a step repeated three times, toluene (20 mL) was added, stirred for 15 min, and then removed under vacuum. The resulting black residue was then treated as in Method A to give dark brown X-ray quality crystals in 62% yield based on Mn. The IR spectrum and magnetic data confirmed the product to be the same as from Method A.

Method C. NaOEt (0.73 mmol, 0.050 g) and $Mn(ClO_4)_2\cdot 6H_2O$ (0.60 mmol, 0.22 g) were added to a stirred solution of solid mpkoH (0.60 mmol, 0.08 g) and Ph_2PO_2H (0.6 mmol, 0.13 g) in EtOH (25 mL). Solid $N^nBu_4MnO_4$ (0.30 mmol, 0.12 g) was added in small portions to the resulting yellow solution, which rapidly darkened and formed a brown precipitate. The slurry was stirred for another 15 min and filtered, and the residue was washed copiously with EtOH. It was then dissolved in hot MeCN and then allowed to cool and concentrate by slow evaporation to give dark brown crystals over 4 d. They were collected by filtration, washed with EtOH and hexane, and dried in vacuum. The yield was 56% based on Mn. The IR spectrum and magnetic data confirmed the product to be the same as from Method A.

$[Mn_3O(O_2PPh_2)_3(ppko)_3](ClO_4)$ (2). $Mn(ClO_4)_2\cdot 6H_2O$ (0.60 mmol, 0.22 g) was added to a stirred solution of solid ppkoH (0.60 mmol, 0.12 g) and Ph_2PO_2H (0.60 mmol, 0.13 g) in CH_2Cl_2/MeOH (25 mL, 4:1 v/v). $N^nBu_4MnO_4$ (0.15 mmol, 0.06 g) was added in small portions to the resulting yellow solution, which rapidly turned deep brown. The solution was stirred for a further 15 min and filtered, and the filtrate was allowed to stand undisturbed at ambient temperature. Dark brown X-ray quality crystals grew over 3 d. They were collected via filtration, washed copiously with CH_2Cl_2, and dried in vacuum. The yield was 63% based on Mn. Calcd (Found) for $\mathbf{2}\cdot 2H_2O$ ($C_{72}H_{61}ClN_6O_{16}P_3Mn_3$): C, 55.45 (55.43); H, 3.94 (3.76); N, 5.39 (4.99)%. Selected IR data (KBr, cm^{-1}): 3441(br), 3054(w), 2068(w), 1596(s), 1482 (s), 1462(s), 1437(s), 1384(s), 1223(m), 1131(m), 1122(m), 1033(m), 1010(m), 992(m), 781(m), 754(m), 728(s), 707(s), 657(s), 636(m), 622(s), 555(m), 529(m), 470(m), 441(w).

$[Mn_6O_2(OMe)_4(O_2PPh_2)_4(mpko)_4](ClO_4)_2$ (3). NaOMe (0.93 mmol, 0.050 g) and $Mn(ClO_4)_2\cdot 6H_2O$ (0.60 mmol, 0.22 g) were added to a stirred solution of mpkoH (0.60 mmol, 0.080 g) and Ph_2PO_2H (0.60 mmol, 0.13 g) in MeOH (25 mL). Solid $N^nBu_4MnO_4$ (0.30 mmol, 0.12 g) was then added in small portions to give a dark brown solution, which was stirred for a further 15 min and filtered, and the filtrate was allowed to stand undisturbed at ambient temperature. Dark brown X-ray quality crystals formed over 3 d, and they were collected via filtration, washed copiously with MeOH, and dried in vacuum. The yield was 64% based on Mn. Calcd (Found) for $\mathbf{3}\cdot 2H_2O$ ($C_{80}H_{84}N_8O_{28}P_4Cl_2Mn_6$): C, 45.11 (45.21); H, 3.97 (3.66); N, 5.26 (4.89)%. Selected IR data (KBr, cm^{-1}): 3436(br), 3056(w), 2935(w), 2871(w), 2067(w), 1604(s), 1555(w), 1477(m), 1384(s), 1298(w), 1277(m), 1247(w), 1156(w), 1130(w), 1107(w), 1037(m), 1016(m), 982(m), 926(s), 827(w), 784(w), 757(s), 726(s), 700(m), 657(s), 623(s), 561(w), 457(w).

$[Mn_9O_6(O_2CMe)_7(O_3PPh)_2(mpko)_3(H_2O)]$ (4). $PhPO_3H_2$ (0.50 mmol, 0.080 g) was added to a stirred solution of $Mn(O_2CMe)_2\cdot 4H_2O$ (1.2 mmol, 0.29 g) and mpkoH (1.2 mmol, 0.16 g) in MeCN/MeOH (21 mL, 1:2 v/v). Solid $N^nBu_4MnO_4$ (0.30 mmol, 0.12 g) was then added in small portions to give a dark brown solution, which was

DOI: 10.1021/acs.inorgchem.7b01793
Inorg. Chem. 2017, 56, 11352−11364

Table 1. Crystallographic Data for Complexes 1, 3, 4, and 5

	1·5CH_2Cl_2	3·2MeOH	4·10MeCN	5
formula[a]	$C_{62}H_{61}Cl_{11}Mn_3N_6O_{14}P_3$	$C_{80}H_{86}Cl_2Mn_6N_6O_{28}P_4$	$C_{67}H_{84}Mn_9N_{16}O_{30}P_2$	$C_{21}H_{29}Cl_3Mn_3N_6O_{20}$
FW, g/mol[a]	1761.85	2103.97	2149.90	956.67
crystal syst	rhombohedral	triclinic	monoclinic	monoclinic
space group	*R*3	$P\bar{1}$	$P2_1/n$	*Pn*
a, Å	15.8065(8)	15.8655(7)	16.4261(7)	16.4817(13)
b, Å	15.8065(8)	17.0134(7)	29.5809(13)	10.4222(8)
c, Å	25.7416(13)	17.3700(8)	17.5671(8)	20.3038(15)
α, deg	90	87.724(1)	90	90
β, deg	90	86.814(1)	98.551(6)	91.919(2)
γ, deg	120	85.585(1)	90	90
volume, Å^3	5569.8(5)	4664.5(4)	8440.9(6)	3485.7(5)
z	3	2	4	4
T, K	100(2)	100(2)	100(2)	100(2)
λ,[b] Å	0.710 73	0.710 73	0.710 73	0.710 73
ρ_{cal}, g/cm^3	1.576	1.498	1.692	1.823
μ, mm^{-1}	1.027	0.991	1.427	1.391
*R*1[c,d]	0.0302	0.0776	0.0926	0.0856
*wR*2[e]	0.0795	0.1631	0.1602	0.1251

[a]Including solvent molecules. [b]Graphite monochromator. [c]$I > 2\sigma(I)$. [d]$R1 = 100\sum(||F_o| - |F_c||)/\sum|F_o|$. [e]$wR2 = 100[\sum[w(F_o^2 - F_c^2)^2]/\sum[w(F_o^2)^2]]^{1/2}$, $w = 1/[\sigma^2(F_o^2) + [(ap)^2 + bp]$, where $p = [\max(F_o^2, 0) + 2F_c^2]/3$.

stirred for a further 1 h and filtered, and the filtrate was layered with acetone/hexane (1:1 v/v). Well-formed, X-ray quality dark brown crystals were obtained over 4 d, and they were collected via filtration, washed copiously with hexane and acetone, and dried in vacuum. The yield was 23% based on Mn. Calcd (Found) for **4** ($C_{47}H_{54}N_6O_{30}P_2Mn_9$): C, 32.24 (32.60); H, 3.33 (2.91); N, 4.70 (4.90)%. Selected IR data (KBr, cm^{-1}): 3393(br), 3123(br), 1605(w), 1557 (s), 1403(s), 1345(s), 1263(s), 1153(s), 1136(s), 1106(s), 1042(s), 980(s), 957(s), 826(m), 781(s), 712(m), 677(s), 646(s), 612(m), 556(s), 502(m), 469(m).

$[Mn_3O(mpko)_3(H_2O)_4(ClO_4)_2](ClO_4)$ (5). To a stirred solution of $Mn(ClO_4)_2·6H_2O$ (6.0 mmol, 2.2 g) in MeCN/MeOH (44 mL, 10:1 v/v) was added NEt_3 (6.0 mmol, 0.84 mL). The resulting light brown slurry was vigorously stirred for 15 min, and then mpkoH (6.0 mmol, 0.80 g) was added to give a dark brown slurry. After it was stirred for a further 2 h, the solvent was removed with a rotary evaporator, the brown residue was dissolved in CH_2Cl_2/MeCN (55 mL, 10:1 v/v) and filtered, and the filtrate was left undisturbed at ambient temperature. Dark brown, X-ray quality crystals grew over 4 d, and they were collected by filtration, washed with CH_2Cl_2, and dried under vacuum. The yield was 17% based on Mn. Calcd (Found) for **5** ($C_{21}H_{29}N_6O_{20}Cl_3Mn_3$): C, 26.36 (25.96); H, 3.06 (2.72); N, 8.78 (8.45)%. Selected IR data (KBr, cm^{-1}): 3436(br), 2070(w), 1604(s), 1479(m), 1384(s), 1108(w), 1040(w), 780 (s), 713(s), 624(s).

X-ray Crystallography. Data were collected at 100 K on a Bruker DUO diffractometer using Mo K*α* radiation (*λ* = 0.710 73 Å) and an APEXII CCD area detector. Raw data frames were read by program *SAINT*[36] and integrated using three-dimensional (3D) profiling algorithms. The data were corrected for Lorentz and polarization effects, and numerical absorption corrections were applied based on indexed and measured faces. The structures were solved using *SHELXTL6.1*, or *SHELXTL2014* for **4**.10MeCN, and refined on F^2 using full-matrix least-squares cycles. The non-H atoms were refined with anisotropic thermal parameters; all H atoms were placed at calculated, idealized positions and refined as riding on their parent atoms. Unit cell and refinement parameters are listed in Table 1.

For **1**·5CH_2Cl_2, the asymmetric unit consists of $^1/_3$ of the Mn_3 cluster and ClO_4^- anion, one CH_2Cl_2 in a general position, and two $^1/_3$ CH_2Cl_2 on threefold axes. Each solvent molecule is disordered and refined in two positions. In the final refinement cycle, 47 496 reflections (of which 5653 were observed with $I > 2\sigma(I)$) were used to refine 324 parameters, and the resulting R_1, wR_2, and *S* (goodness of fit) were 2.98%, 7.93%, and 1.061, respectively.

For **3**·2MeOH, the asymmetric unit consists of two $^1/_2$ Mn_6 clusters (A and B), two ClO_4^- anions, and two MeOH molecules. In both clusters, the $mpko^-$ ligands show some disorder, as do both ClO_4^- anions, which were each refined at two sites. The MeOH molecules were badly disordered and could not be modeled properly; thus, program SQUEEZE,[37] a part of the PLATON[38] package of crystallographic software, was used to calculate the solvent disorder area and remove its contribution to the overall intensity data. In the final cycle of refinement, 21 359 reflections (of which 16 673 were observed with $I > 2\sigma(I)$) were used to refine 1130 parameters, and the resulting R_1, wR_2, and *S* were 6.09%, 15.49%, and 1.030, respectively.

For **4**·10MeCN, the asymmetric unit consists of the Mn_9 cluster and 10 MeCN molecules. The latter were disordered and could not be modeled properly; thus, program SQUEEZE was again used. The bound H_2O protons were obtained from a difference Fourier map and refined as riding on their parent O atoms. In the final cycle of refinement, 19 294 reflections (of which 13 623 are observed with $I > 2\sigma(I)$) were used to refine 857 parameters, and the resulting R_1, wR_2, and *S* were 6.16%, 15.06%, and 1.025, respectively.

For **5**, the asymmetric unit consists of two Mn_3 clusters (A and B) and two ClO_4^- anions. In Mn_3 cluster B, the ClO_4^- bound to Mn1B is disordered and was refined in two parts. One ClO_4^- anion (Cl3B) was also disordered and refined in two parts. All bound H_2O protons were located in difference Fourier maps and were refined riding on their parent O atoms. Owing to the number of cations and anions in the asymmetric unit, a search for higher symmetry ($P2_1/n$) was performed, but none was found. A closer look at the asymmetric unit revealed the absence of inversion symmetry, thus confirming the correct space group as *Pn*. In the final cycle of refinement, 15 769 reflections (of which 11 210 were observed with $I > 2\sigma(I)$) were used to refine 956 parameters, and the resulting R_1, wR_2, and *S* were 5.54%, 11.73%, and 0.961, respectively.

Other Studies. Elemental analyses (C, H, N) were performed by the in-house facilities of the University of Florida Chemistry Department or Complete Analysis Laboratories, Inc. Infrared spectra in the 400−4000 cm^{-1} range were recorded on KBr pellets using a Nicolet Nexus 670 FTIR spectrometer. Variable-temperature direct-current (dc) and alternating-current (ac) magnetic susceptibility data were collected on vacuum-dried solids using a Quantum Design MPMS-XL SQUID magnetometer equipped with a 7 T magnet and operating in the 1.8−300 K range. Microcrystalline samples were restrained in solid eicosane to prevent torqueing. Magnetization versus field and temperature data were fit using the program MAGNET.[39]

DOI: 10.1021/acs.inorgchem.7b01793
Inorg. Chem. 2017, 56, 11352−11364

Pascal's constants[40] were used to estimate the diamagnetic corrections, which were subtracted from the measured susceptibilities to give the molar paramagnetic susceptibility (χ_M).

RESULTS AND DISCUSSION

Syntheses. $[Mn_3O(O_2PPh_2)_3(mpko)_3](ClO_4)$ (**1**; $3Mn^{III}$) was obtained in 88% yield from the reaction of Ph_2PO_2H with $[Mn_3O(O_2CMe)_3(mpko)_3](ClO_4)$ (**6**) in a 3:1 molar ratio in CH_2Cl_2/MeCN (eq 1); the CH_2Cl_2 helps dissolve the Ph_2PO_2H. The low pK_a (2.32) of Ph_2PO_2H

$$[Mn_3O(O_2CMe)_3(mpko)_3]^+ + 3Ph_2PO_2H \rightarrow [Mn_3O(O_2PPh_2)_3(mpko)_3]^+ + 3MeCO_2H\uparrow \quad (1)$$

drives the displacement of $MeCO_2H$ (4.76), but to ensure complete reaction the latter was removed as its toluene azeotrope under reduced pressure.[41] **1** could also be obtained more conveniently, but in lower yields of 55−65%, from the reaction of $[Mn_3O(O_2CMe)_6(py)_3](ClO_4)$[35] with mpkoH/$Ph_2PO_2H$ (Method B) or in one step from a comproportionation reaction in EtOH using simple $Mn(ClO_4)_2$/mpkoH/Ph_2PO_2H/NaOEt/MnO_4^- reagents (Method C).

$[Mn_3O(O_2PPh_2)_3(ppko)_3](ClO_4)$ (**2**; $3Mn^{III}$) was also synthesized from a comproportionation reaction, in this case $Mn(ClO_4)_2$/ppkoH/Ph_2PO_2H/MnO_4^- in CH_2Cl_2/MeOH. We wondered whether the bulkier ppkoH might give a different type of product, and although we could not obtain crystals suitable for X-ray crystallography, the elemental analysis, IR spectrum, and magnetic data established **2** to be isostructural with **1**. Small changes in the amount of ppkoH or Ph_2PO_2H employed also gave **2** in comparable yield. In contrast, when Method C to **1** was instead performed with NaOMe and MeOH, the higher nuclearity $[Mn_6O_2(OMe)_4(O_2PPh_2)_4(mpko)_4](ClO_4)_2$ (**3**; $6Mn^{III}$) was obtained, corresponding approximately to a "dimerization" of **1** by formation of MeO^- bridges (vide infra).

We also investigated the use of $PhPO_3H_2$ instead of Ph_2PO_2H. Both the carboxylate substitution reaction with $[Mn_3O(O_2CMe)_3(mpko)_3](ClO_4)$ and the $Mn(ClO_4)_2$/MnO_4^-/mpkoH/$PhPO_3H_2$ comproportionation reaction gave the same insoluble material we assume is polymeric. However, after some additional experimentation, the $Mn(O_2CMe)_2$/MnO_4^-/mpkoH/$PhPO_3H_2$ reaction in a 12:3:12:5 molar ratio led to $[Mn_9O_6(O_2CMe)_7(O_3PPh)_2(mpko)_3(H_2O)]$ (**4**; Mn^{II}, $8Mn^{III}$) in 23% yield. The same product was obtained with Mn^{III} acetate instead of $Mn(O_2CMe)_2$.

Finally, as a control we omitted both Ph_2PO_2H and $PhPO_3H_2$, and the $Mn(ClO_4)_2$/mpkoH/NEt_3 reaction in MeCN/MeOH in a 1:1:1 molar ratio gave the unusual triangular $[Mn_3O(mpko)_3(H_2O)_4(ClO_4)_2](ClO_4)$ (**5**; Mn^{II}, $2Mn^{III}$) in 17% yield. Various attempts to raise the yield by changing the reagent ratios proved unsuccessful. The synthesis is summarized in eq 2.

$$3Mn^{2+} + 3mpkoH + 2ClO_4^- + 0.5O_2 + 4H_2O \rightarrow [Mn_3O(mpko)_3(H_2O)_4(ClO_4)_2]^+ + 3H^+ \quad (2)$$

Description of Structures. The cation of **1** and its core are shown in Figure 1; selected distances and angles are listed in Table S1. The complex crystallizes in space group $R\bar{3}$ and contains an equilateral Mn^{III}_3 triangle bridged by a central μ_3-O^{2-} that is 0.298 Å out of the Mn_3 plane. Each Mn_3 edge is bridged by both a $Ph_2PO_2^-$ and an $mpko^-$, the latter in its chelating/bridging mode. The Mn are six-coordinate with distorted, axially elongated octahedral geometry characteristic of the Jahn−Teller (JT) distortion of high-spin Mn^{III} (green axes in Figure 1). The Mn^{III} oxidation states were confirmed by bond valence sum (BVS) calculations (Table S2).

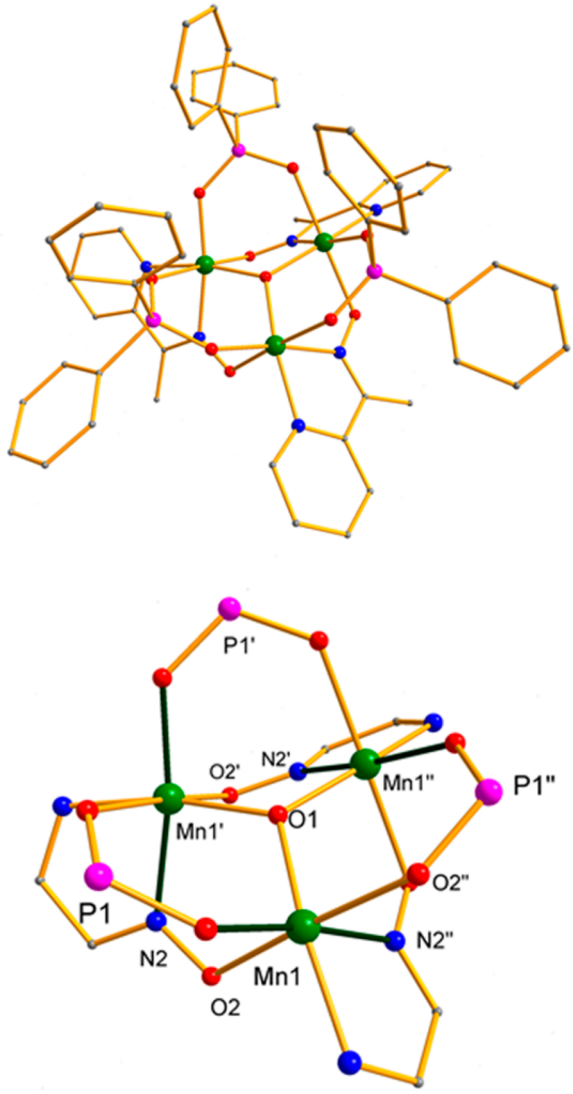

Figure 1. (a) Complete structure of the cation of **1** and (b) a partially labeled structure of the core. Primed and unprimed atoms are related by crystallographic C_3 symmetry, and the Mn^{III} JT elongation axes are along the thick dark green bonds. Color code: Mn^{III} green, P violet, N blue, O red, C gray. H atoms were omitted for clarity.

Comparisons between **1** and $[Mn_3O(O_2CR)_3(mpko)_3](ClO_4)$ (R = Me (**6**), Et (**7**), and Ph (**8**))[31] reveal that the bulkier $Ph_2PO_2^-$ versus RCO_2^- ligands caused only minor structural distortions (Table 2). As for **6**−**8**, the $Ph_2PO_2^-$ and $mpko^-$ ligands are on opposite sides of the Mn_3 plane. **1** has slightly longer average Mn···Mn separations than **6**−**8** (which, unlike **1**, do not lie on crystallographic C_3 axes and thus exhibit their intrinsic isosceles nature) and larger Mn−N−O-Mn torsion angles (ψ). However, the distance of the μ_3-O^{2-} in **1** out of the Mn_3 (0.298 Å) plane is almost the same as in **6**−**8** (0.286−0.294 Å). The resulting conclusion that the bulkier $Ph_2PO_2^-$ with its two Ph rings caused little structural distortion versus RCO_2^- is evident in the space-filling representation of **1**

DOI: 10.1021/acs.inorgchem.7b01793
Inorg. Chem. 2017, 56, 11352−11364

Table 2. Comparison of Structural and Magnetic Data in Triangular Mn_3 Oximates

parameter	1	2	5[a]	6	7	8
Mn···Mn[b]	3.250[c]		3.163/3.187[c]	3.191[d]	3.197[d]	3.212[d]
	3.250		3.394/3.374	3.193	3.207	3.200
	3.250		3.443/3.407	3.203	3.210	3.219
average	3.250		3.333/3.323	3.196	3.205	3.210
ψ[e]	16.1		11.6/12.6	10.1	9.6	15.4
	16.1		3.7/1.3	12.5	10.1	14.2
	16.1		9.1/10.9	10.9	12.2	9.6
average	16.1		8.1/8.3	11.2	10.6	13.1
d[f]	0.298		0.098/0.041	0.294	0.293	0.286
spin S	6	6	$^5/_2$	6	6	6
g factor	1.94	1.93	1.99	1.92	1.93	1.99
D[g]	−0.29	−0.38	−1.41	−0.34	−0.34	−0.35

[a]Two independent molecules. [b]Angstroms. [c]esd = 0.001 Å. [d]esd = 0.002 Å. [e]Mn−N−O−Mn torsion angle (deg); listed in the same order as the corresponding Mn···Mn distance. [f]Distance (Å) of oxide O atom from the Mn_3 plane. [g]Axial zfs parameter; ±0.02 cm^{-1} except for **5** (±0.04 cm^{-1}).

(Figure S1) that shows that the two Ph groups are well-accommodated without noticeable steric hindrance.

The cation of **3** and its core are shown in Figure 2; selected distances and angles are listed in Table S3. The complex

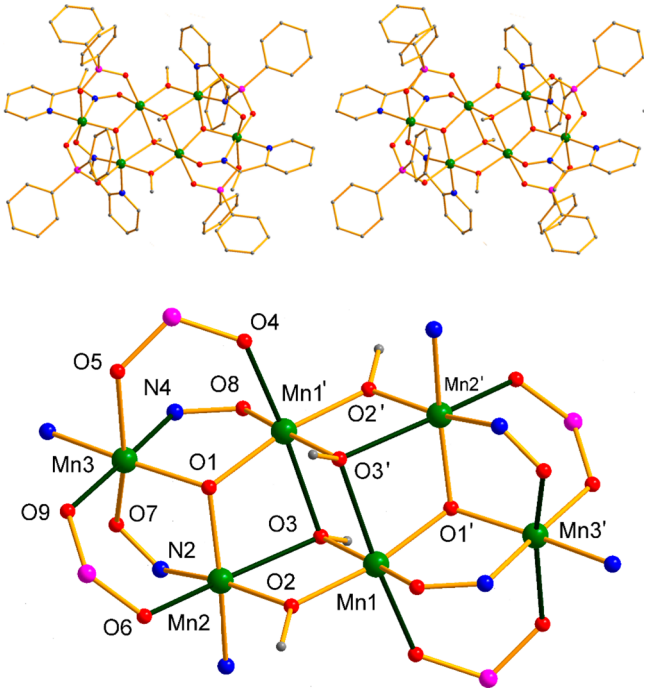

Figure 2. (top) A stereopair of the complete cation of **3**. (bottom) Its labeled core with Mn^{III} JT elongation axes shown as dark green bonds. Primed and unprimed atoms are related by the inversion center. Color code: Mn^{III} green; P violet; O red; N blue; C gray. H atoms were omitted for clarity.

crystallizes in space group $P\bar{1}$, with the asymmetric unit containing two Mn_6 cations (A and B) lying on inversion centers; only one will be described here. All Mn are Mn^{III}, as confirmed by BVS calculations (Table S1), and exhibit JT elongation axes (thicker green bonds in Figure 2). The core is an $[Mn_6(\mu_3\text{-}O)_2(\mu_3\text{-}OMe)_2(\mu_2\text{-}OMe)_2]^{10+}$ unit comprising four edge-fused oxo-capped Mn_3 triangles in a row. The four remaining Mn_2 edges are each bridged by one $Ph_2PO_2^-$ and one $mpko^-$ group in the same bridging modes as in **1**. In fact, **3** can be described as the linkage of two cations of **1** by removing the $Ph_2PO_2^-$ and $mpko^-$ ligands from one edge of each and then joining the edges together with four μ_2 or μ_3 MeO^- groups to give the complete $[Mn_6O_2(OMe)_4(O_2PPh_2)_4(mpko)_4]^+$.

4 and its core are shown in Figure 3; selected distances and angles are listed in Table S4. The cluster crystallizes in space group $P2_1/n$ with no crystallographic symmetry. The Mn_9 unit comprises three $Mn_5/Mn_3/Mn$ layers giving a distorted pyramidal topology, with the Mn^{II} at the apex, held together by six μ_3-O^{2-} ions. The Mn oxidation states were confirmed by BVS calculations (Table S2). The two $PhPO_3^{2-}$ groups bridge on side faces of the pyramid in different μ_5 modes (Figure 3, bottom), giving a $\{Mn_9O_6(O_3PPh)_2\}$ cagelike core. The remaining ligation is provided by seven $MeCO_2^-$, three $mpko^-$, and one H_2O molecule. Six $MeCO_2^-$ bind in their usual $\eta^1{:}\eta^1{:}\mu_2$ mode, and the seventh is bound terminally to Mn3. The three $mpko^-$ are in the usual chelating/bridging modes, while the lone H_2O ligand is bound terminally to Mn8. Mn3 and Mn7 are five-coordinate with square-pyramidal geometry (τ = 0.23 and 0.01, respectively), while the rest are six-coordinate and JT-distorted (thick green bonds in Figure 3, middle). All JT axes involve a phosphonate and a carboxylate O atom. Examination of the packing shows that the unbound O atom (O19) of the terminal $MeCO_2^-$ of one Mn_9 is hydrogen-bonded to the H_2O ligand (O30) of a neighboring molecule (O30−H···O19 = 2.714(6) Å) to give a one-dimensional (1D) chain (Figure S2).

The cation of **5** and its core are shown in Figure 4; selected distances and angles are listed in Table S5. The complex crystallizes in space group *Pn*, with two molecules (A and B) in the asymmetric unit, and contains a triangular $Mn^{II}Mn^{III}_2$ core (Table S2) bridged by a central μ_3-O^{2-}, which is almost coplanar (0.098 and 0.041 Å for A and B, respectively, out of the Mn_3 plane).

Each Mn_2 edge is has a chelating/bridging $mpko^-$, and ligation is completed by four terminal H_2O and two terminal ClO_4^-. Two H_2O ligands are *trans* on the Mn^{II} (Mn3), and the Mn^{III} each have a *trans* H_2O/ClO_4^- pair. The Mn^{III} JT axes (dark green bonds in Figure 4) are essentially parallel. As expected, there is extensive $HOH\cdots OH_2$ and $HOH\cdots OClO_3^-$ hydrogen bonding either directly between the cations or between a cation and a ClO_4^- anion, giving a 3D network. Fortunately, none are $Mn^{III}{-}H_2O\cdots H_2O{-}Mn^{III}$, so intercation exchange interactions should be very weak (vide infra). The large number of weak H_2O and ClO_4^- ligands in **5** somewhat

DOI: 10.1021/acs.inorgchem.7b01793
Inorg. Chem. 2017, 56, 11352−11364

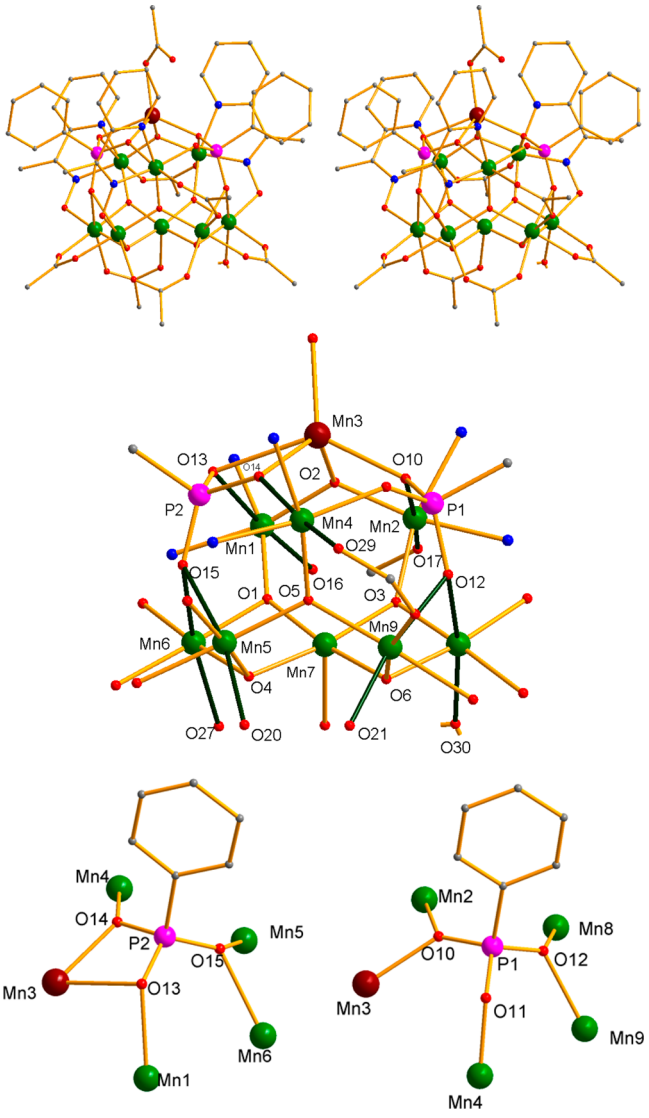

Figure 3. (top) A stereopair of the complete structure of **4**. (middle) Its labeled core with Mn^{III} JT elongation axes shown as dark green bonds. (bottom) The two μ_5-$PhPO_3^{2-}$ groups showing the difference in their binding modes. Color code: Mn^{III} green; Mn^{II} brown; P violet; O red; N blue; C gray. H atoms were omitted for clarity.

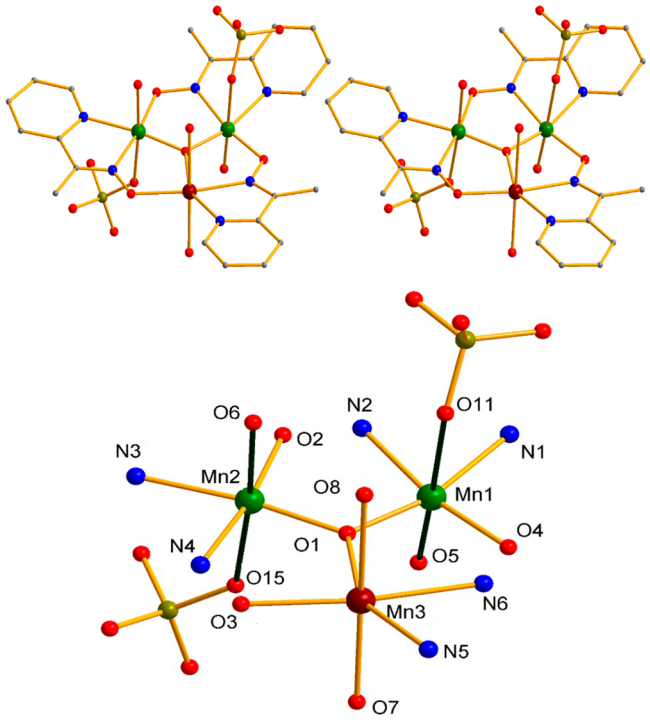

Figure 4. (top) A stereopair of the complete structure of molecule A of **5** and (bottom) its labeled core with Mn^{III} JT elongation axes shown as dark green bonds. Color code: Mn^{III} green; P violet; O red; N blue; C gray. H atoms were omitted for clarity.

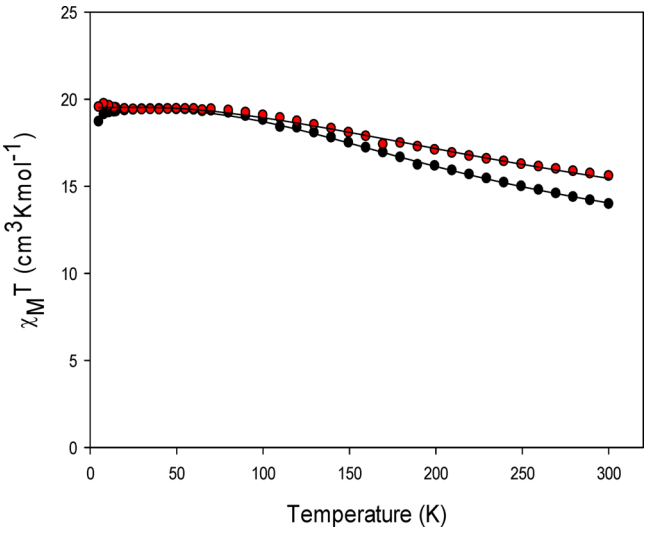

Figure 5. $\chi_M T$ vs T plots for $1{\cdot}H_2O$ (black ●) and $2{\cdot}2H_2O$ (red ●). Solid lines are fits of the experimental data; see the text for the fit parameters.

rationalizes the low yield of what is undoubtedly a very reactive molecule; in fact, it is probably due to the stabilizing influence of the extensive hydrogen bonding in the solid state that any **5** could be isolated.

Magnetochemistry. Direct-Current Magnetic Susceptibility Studies. Solid-state, dc magnetic susceptibility (χ_M) data were collected on powdered microcrystalline samples of $1{\cdot}H_2O$, $2{\cdot}2H_2O$, $3{\cdot}2H_2O$, **4**, and **5**, restrained in eicosane to prevent torquing, in the 5.0–300 K range in a 0.1 T field.

For $1{\cdot}H_2O$ and $2{\cdot}2H_2O$, the data are shown in Figure 5. $\chi_M T$ for $1{\cdot}H_2O$ increases steadily from 13.91 cm^3 mol^{-1} K at 300 K to a plateau of 19.44 cm^3 K mol^{-1} below 35 K and then decreases very slightly below 10 K to 19.14 cm^3 K mol^{-1} at 5.0 K. The increasing $\chi_M T$ with decreasing T indicates intramolecular ferromagnetic (**F**) interactions. $2{\cdot}2H_2O$ exhibits a similar profile, increasing from 15.63 cm^3 mol^{-1} K at 300 K to the same plateau of 19.44 cm^3 K mol^{-1} below 35 K. The plateaus and their values indicate a well-isolated $S = 6$ ground state for both complexes, with $g < 2$ slightly as expected for Mn^{III}.

To obtain the Mn···Mn exchange parameters (J), the $\chi_M T$ versus T data were fit to the Van Vleck[42] expression for a Mn^{III}_3 equilateral triangle.[35] The 1-J isotropic Heisenberg–Dirac–Van Vleck (HDVV) spin Hamiltonian is given by eq 3, whose eigenvalues are given by eq 4, where

$$\mathcal{H} = -2J(\hat{S}_1{\cdot}\hat{S}_3 + \hat{S}_2{\cdot}\hat{S}_3 + \hat{S}_1{\cdot}\hat{S}_2) \quad (3)$$

DOI: 10.1021/acs.inorgchem.7b01793
Inorg. Chem. 2017, 56, 11352–11364

$$E(S_T) = -J[S_T(S_T + 1)] \quad (4)$$

S_T is the total spin. Only data greater than 10 K were employed to avoid the lower-T effects from zero-field splitting (zfs), intermolecular interactions, etc. Good fits (solid lines in Figure 5) were obtained with J = 16.0(1) cm^{-1} and g = 1.94(1) for **1**·H_2O, and J = 16.4(1) cm^{-1} and g = 1.92(1) for **2**·2H_2O, with temperature-independent paramagnetism (TIP) kept constant at 600 × 10^{-6} cm^3 mol^{-1}. The obtained J values indicate the S = 5 first excited state to be 192(1) and 197(1) cm^{-1}, respectively, above the S = 6 ground state.

The successful fits above to an equilateral model contrast with those for the carboxylate analogues **6**–**8**, for which only a 2-J isosceles triangle model gave good fits, consistent with their isosceles structures.[31] **1** has crystallographic C_3 symmetry (**6**–**8** do not), so even though the crystallographic symmetry could be masking lower symmetry at each molecule, we suspected that **1** might nevertheless be closer to a true equilateral triangle than **6**–**8**. Fitting the data in Figure 5 to an isosceles model[31] gave J_a = 15.3(4.6) cm^{-1}, J_b = 17.4(10.0) cm^{-1}, and g = 1.94(1), where J_b refers to the unique edge. The average of the three values is J = 16.0 cm^{-1}, identical to the 1-J fit. The similar J_a and J_b for **1** can be compared with J_a = 12.1–18.6 cm^{-1} and J_b = 1.5–6.7 cm^{-1} for **6**–**8**, consistent with their degree of distortion from equilateral, and suggesting **1** may indeed be structurally very close to equilateral. The very "soft" fits, that is, high uncertainties in J_a and J_b, are also assigned to this, namely, a wide range of J_a/J_b will give a good fit as long as their average is 16.0 cm^{-1}. We speculate that the larger organic groups surrounding the core in **1** and **2** help buffer the cores from packing forces, etc., and minimize distortion. Note that, for these ferromagnetic Mn^{III}_3 systems with a singly degenerate S = 6 ground state, distortions arising from spin frustration and magnetic Jahn–Teller effects, as arise from the electronic structure of antiferromagnetic equilateral triangles, are inoperative.[43]

To determine the axial zfs parameter (D) for **1**·H_2O and **2**·2H_2O, magnetization (M) data were collected in the 0.1–7.0 T and 1.8–10.0 K ranges, and they are plotted in Figure 6 as $M/N\mu_B$ versus H/T, where N is Avogadro's number, μ_B is the Bohr magneton, and H is the applied field. The data were fit, using program *MAGNET*,[39] by diagonalization of the spin Hamiltonian matrix assuming only the ground state is populated, incorporating axial anisotropy ($D\hat{S}_z^2$) and Zeeman terms, and employing a full powder average. The spin Hamiltonian is given by eq 5, where μ_0 is the vacuum permeability. Excellent fits (solid lines in Figure 6) were obtained with S = 6, g = 1.94(1),

$$\mathcal{H} = D\hat{S}_z^{\ 2} + g\mu_B\mu_0\hat{S}\cdot H \quad (5)$$

and D = −0.29(2) cm^{-1} for **1**·H_2O, and S = 6, g = 1.99(1), and D = −0.38(2) cm^{-1} for **2**·2H_2O. All data up to 7 T were used, consistent with a well-isolated ground state, which precludes problems in high fields from low-lying excited states. Comparison of the D values for **1** and **2** with those for **6**–**8** (Table 2) shows that they are very similar, within uncertainties. Therefore, the similar core structures of **1**/**2** and **6**–**8** lead in both cases to **F** coupling, S = 6 ground states, and very similar D values. Thus, small differences to metric parameters and molecular symmetry notwithstanding, the $Ph_2PO_2^-$ groups proved good replacements for RCO_2^- groups, despite their greater bulk and different electronic properties.

For **3**·2H_2O, $\chi_M T$ decreases slowly with decreasing T from 17.98 cm^3 K mol^{-1} at 300 K and then more steeply below 100 K, reaching 8.68 cm^3 K mol^{-1} at 5.0 K (Figure 7, top). This profile indicates dominant antiferromagnetic (**AF**) interactions that are weak, and the $\chi_M T$ at 5.0 K suggests an S = 4 ground state with g < 2; the spin-only (g = 2) $\chi_M T$ for S = 3, 4, and 5 are 6.0, 10.0, and 15.0 cm^3 K mol^{-1}, respectively. The slow decrease in $\chi_M T$ indicates weak couplings, which together with the complexity and low symmetry of **3** makes it very challenging to determine the various pairwise J couplings. We thus concentrated on determining the ground-state properties.

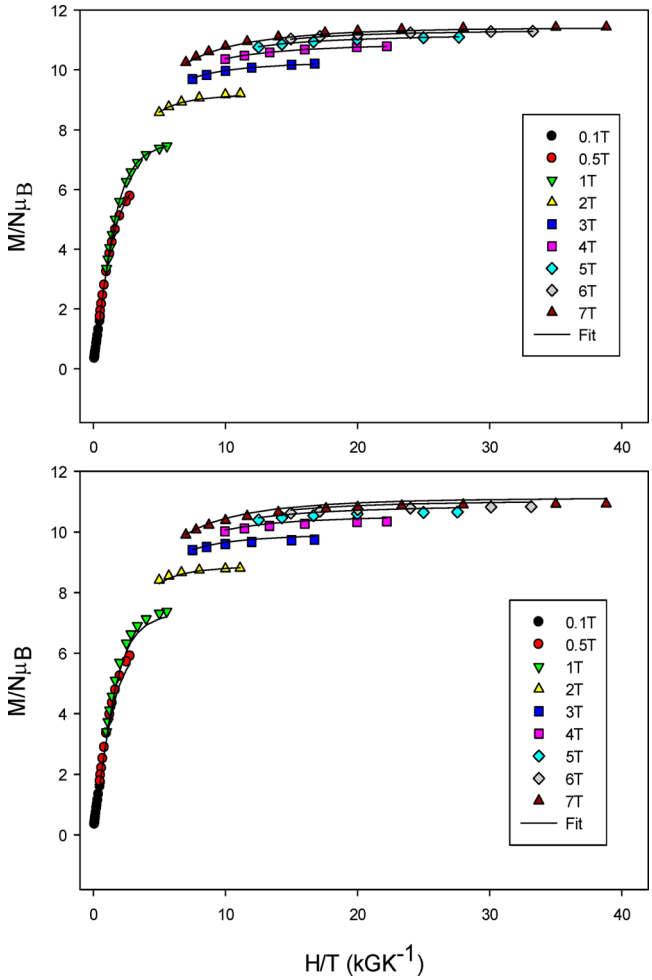

Figure 6. Reduced magnetization ($M/N\mu_\beta$) vs H/T plots for (top) **1**·H_2O and (bottom) **2**·2H_2O at the indicated dc fields. The solid lines are the fit of the data; see the text for the fit parameters.

No satisfactory fit of $M/N\mu_B$ versus H/T data in the 0.1–7.0 T and 1.8–10.0 K ranges could be obtained. Given the weak **AF** couplings, we suspected field-induced problems from low-lying excited states with S greater than the ground state. To avoid these, we progressively removed data at high fields, and a good fit was obtained with S = 4, g = 1.96(1), and D = −0.29(2) cm^{-1} using data collected at less than or equal to 3 T (solid lines in Figure 7, bottom). When even just the 4 T data were included, the fit became poor (Figure S4), as low-lying excited states with S > 4 get populated (as their energy is lowered by the applied field), increasing M.

Several Mn^{III}_6 clusters with S = 4 ground states are known among the family of formula $[Mn_6O_2(X\text{-}sao)_6(O_2CR)_2(solv)_n]$ (H-saoH$_2$ = salicylaldoxime; X = H, Me, Et; R = alkyl or aryl; and solv = H_2O, MeOH, or EtOH; n = 4–6).[44] Their ground-state spin ranges from S = 4–12, depending on R and the

DOI: 10.1021/acs.inorgchem.7b01793
Inorg. Chem. 2017, 56, 11352–11364

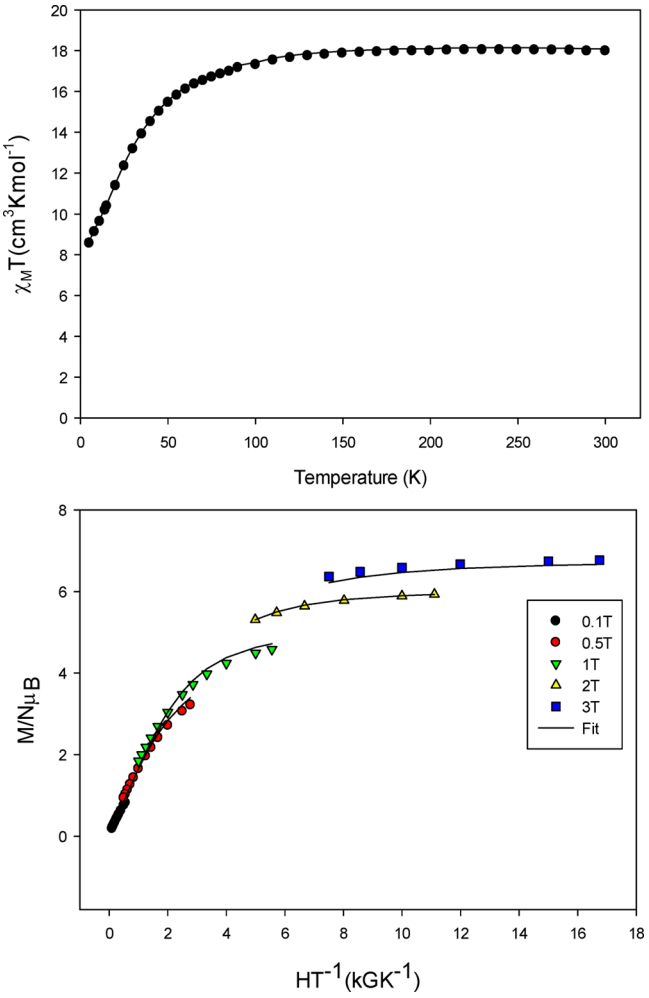

Figure 7. (top) $\chi_M T$ vs T plot for **3**·2H_2O and (bottom) reduced magnetization ($M/N\mu_\beta$) vs H/T plots at the indicated dc fields, with the fit shown as solid lines; see the text for the fit parameters.

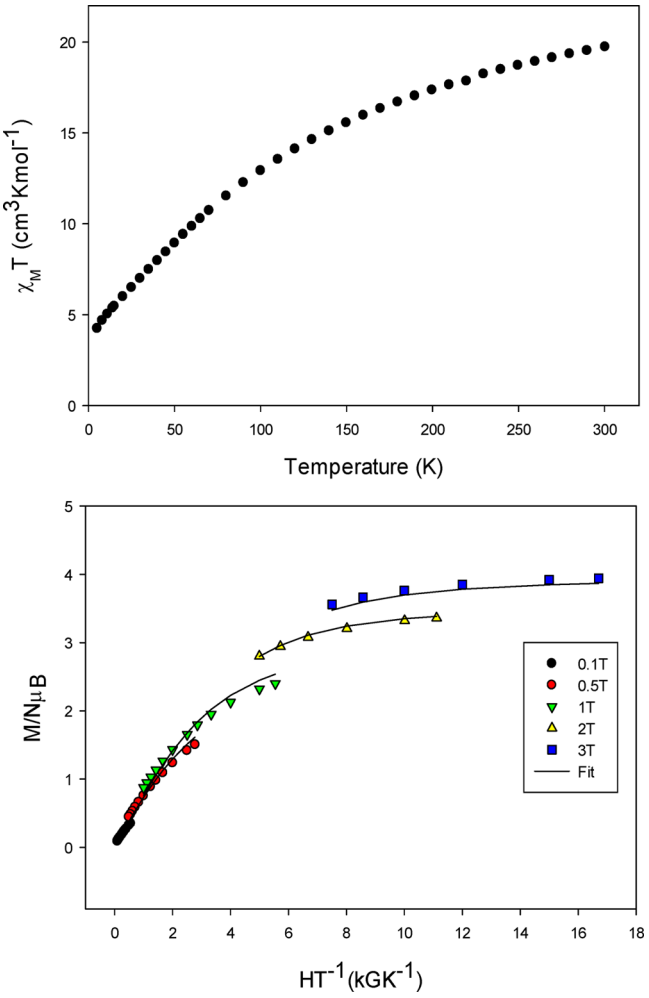

Figure 8. (top) $\chi_M T$ vs T plot for **4**, and (bottom) reduced magnetization ($M/N\mu_\beta$) vs H/T plots at the indicated dc fields, with the fit shown as solid lines; see the text for the fit parameters.

oximate torsion angles. **3** is related to this family in that its core is the linkage of two triangular Mn_3O units. The Mn−O−N−Mn torsion angles in **3**·2H_2O (14.95° and 5.82°) are well-below the value of 31° empirically determined to be needed in this Mn_6 family to switch from dominant **AF** to **F** interactions and a resulting S = 12 ground state.[44a]

For **4**, $\chi_M T$ decreases steadily from 19.73 cm^3 K mol^{-1} at 300 K to 4.25 cm^3 K mol^{-1} at 5.0 K (Figure 8) indicating dominant **AF** interactions. The $\chi_M T$ at 5.0 K suggests an $S = {}^5/_2$ ground state; the spin-only $\chi_M T$ for $S = {}^3/_2$, ${}^5/_2$, and ${}^7/_2$ are 1.9, 4.4, and 7.9 cm^3 K mol^{-1}, respectively. Given the complexity of **4**, we again concentrated on characterizing its ground state. Using all M data collected in the 0.1−7.0 T and 1.8−10.0 K ranges gave no satisfactory fit, but using only data at less than or equal to 3 T gave a good fit (solid lines in Figure 8) with $S = {}^5/_2$, g = 1.99(2), and D = −1.26(4) cm^{-1}. As for **3**, including even just the 4 T data gave a poor fit (Figure S4).

To assess the precision of the large value of D, the root-mean-square error surface for the D versus g fit was calculated using the program *GRID*[45] and is shown as a two-dimensional (2D) contour plot in Figure S5. The fit is only somewhat soft with respect to both g and D, expressed as the resulting precision uncertainties in these parameters above, and we conclude that **4** does have a large D, which is consistent with a combination of small S and the near-parallel orientation of several JT axes to give a large molecular D value. **4** joins a growing list of 3d metal phosphonate clusters[46] and is the third at the Mn_9 nuclearity.[47] One of the previous examples, $[Mn_9Na(\mu_3\text{-}O)_4(\mu_4\text{-}O)_2(O_3PPh)_2(O_2CBu^t)_{12}\text{-}(H_2O)_2(H_2O)_{0.67}(py)_{0.33}]$, has a Mn_9 subunit similar to that of **4**, but otherwise is very different in that it is heterometallic, all-Mn^{III}, contains no oximates or other chelates, and has an S = 8 ground state.

For **5**, $\chi_M T$ decreases steadily from 10.63 cm^3 K mol^{-1} at 300 K to 4.26 cm^3 K mol^{-1} at 5.0 K (Figure 9, top) indicating dominant **AF** interactions and an $S = {}^5/_2$ ground state. The data were fit to the Van Vleck expression for a $Mn^{II}Mn^{III}_2$ isosceles triangle.[31] The 2-J HDVV spin Hamiltonian is given by eq 6, whose eigenvalues are given by eq 7, where $\hat{S}_A = \hat{S}_1 + \hat{S}_2$ and $\hat{S}_T = \hat{S}_A + \hat{S}_3$. J_a

$$\mathcal{H} = -2J_a(\hat{S}_1\cdot\hat{S}_3 + \hat{S}_2\cdot\hat{S}_3) - 2J_b\hat{S}_1\cdot\hat{S}_2 \quad (6)$$

$$E(S_T, S_A) = -J_a[S_T(S_T + 1) - S_A(S_A + 1)] - J_b[S_A(S_A + 1)] \quad (7)$$

and J_b are defined in the inset to Figure 9, top, $S_1 = S_2 = 2$, and $S_3 = {}^5/_2$. $E(S_T, S_A)$ is the energy of state S_T arising from S_A. The fit (solid line in Figure 9) gave J_a = −0.67(2), J_b = −4.30(6),

DOI: 10.1021/acs.inorgchem.7b01793
Inorg. Chem. 2017, 56, 11352−11364

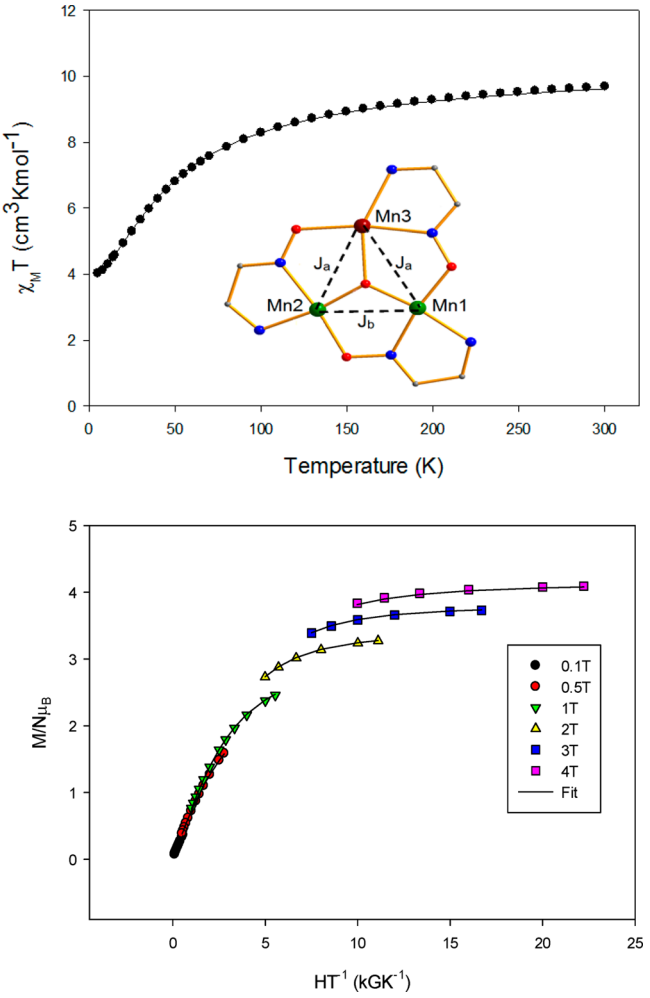

Figure 9. (top) $\chi_M T$ vs T plot for **5**. The solid line is the fit to the 2-J isosceles model defined in the inset. (bottom) Reduced magnetization ($M/N\mu_\beta$) vs H/T plots at the indicated dc fields, with the fit shown as solid lines. See the text for both sets of fit parameters.

and g = 1.98(1), with TIP = 450 × 10^{-6} cm^3 mol^{-1}. The ground state is $S = {}^5/_2$, the $|S_T, S_A\rangle = |{}^5/_2, 0\rangle$ state. With $|J_b/J_a| = 6.4$, the two Mn^{III} spins are paired by J_b at low T (i.e., $S_A = 0$), and the ground state is given by the Mn^{II} spin. An $S = {}^5/_2$ ground state for a $Mn^{II}Mn^{III}_2$ isosceles triangle with each Mn···Mn edge bridged by identical ligands is unprecedented. In previous examples, such mixed-valence Mn_3 clusters have possessed $S = {}^1/_2$ or ${}^3/_2$ ground states, as expected for spin-frustrated systems where the J_a and J_b are more comparable in magnitude;[48] as stated, it is the large $|J_b/J_a| = 6.4$ that leads to the $S = {}^5/_2$ ground state for **5**.

Fits of $M/N\mu_B$ versus H/T data were acceptable only if data at less than or equal to 4 T were employed (solid lines in Figure 9, bottom) indicating low-lying excited states with $S > {}^5/_2$. The fit parameters were $S = {}^5/_2$, g = 1.98(2), and D = −1.41(4) cm^{-1}. Inclusion of data at 5 T gives a poor fit (Figure S6). The large D value is consistent with the structure: (i) the weak nature of the ligands (H_2O and ClO_4^-) on the Mn^{III} JT axes leads to particularly long JT elongations (Mn−O = 2.202(5)−2.514(5) Å) that will lead to significant single-ion anisotropy; (ii) although **5** only has two Mn^{III}, their JT axes are almost parallel, which is expected to give a significant molecular D; and (iii) the spin is small, which should favor a larger D value. The D versus g error surface (Figure S7) supports the large D value and provides the fit uncertainties. The data for **5** are also consistent with the even larger D values (ca. −2.3 cm^{-1}) reported for some similarly near-planar Mn^{III}_3 triangles with sao^{2-} ($saoH_2$ = salicylaldoxime) chelates, three near-parallel JT axes, **AF** couplings, and S = 2 ground states.[49]

Alternating Current Magnetic Susceptibility Studies. The ac susceptibility data were collected on vacuum-dried samples in the 1.8−15 K range in a 3.5 G ac field at oscillation frequencies up to 1000 Hz.

For **1**·H_2O, **2**·2H_2O, and **5**, the in-phase $\chi'_M T$ versus T data provide independent confirmation of the ground states deduced from the dc studies, with near-plateau values of ∼20, ∼20, and ∼4 cm^3 K mol^{-1}, respectively, consistent with S = 6, 6, and ${}^5/_2$ ground states with g < 2 (Figure 10). Below ∼4 K, **1**·H_2O and

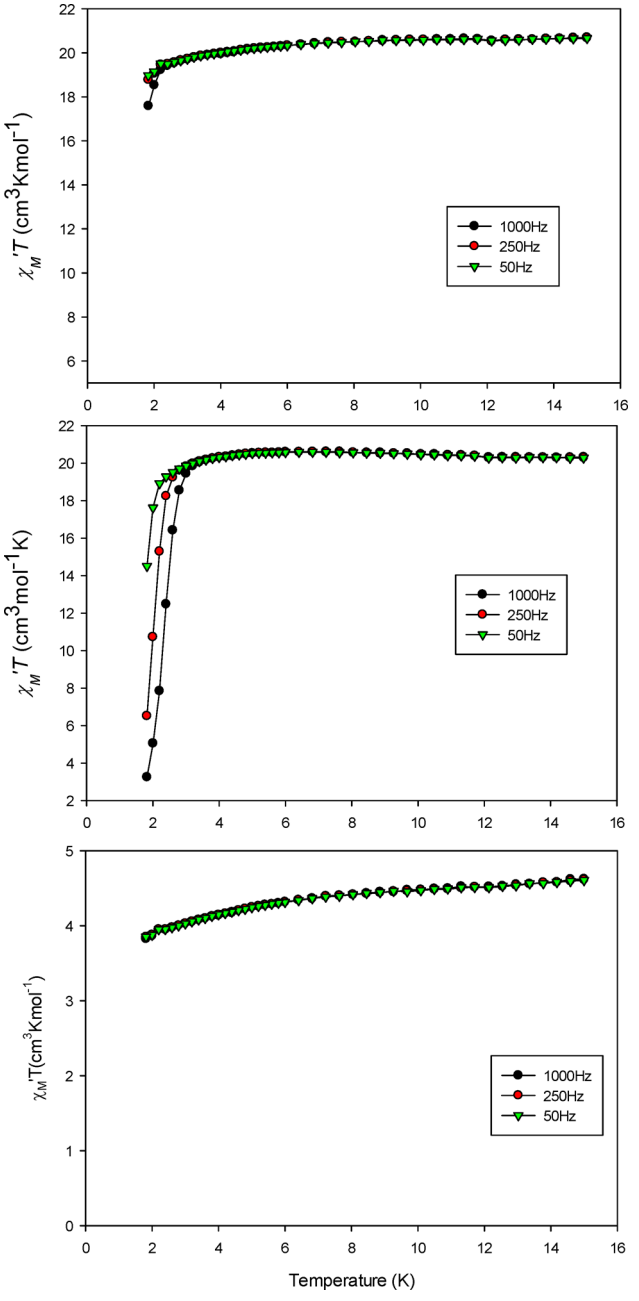

Figure 10. In-phase ac $\chi'_M T$ vs T at the indicated frequencies for (top) **1**·2H_2O, (middle) **2**·H_2O, and (bottom) **5**. The solid lines are guides for the eye.

DOI: 10.1021/acs.inorgchem.7b01793
Inorg. Chem. 2017, 56, 11352−11364

2·2H_2O show the frequency-dependent decreases due to the slow magnetization relaxation of SMMs, and out-of-phase χ_M'' are observed (Figure 11). χ'_MT for **3**·2H_2O and **4** are ∼9 and

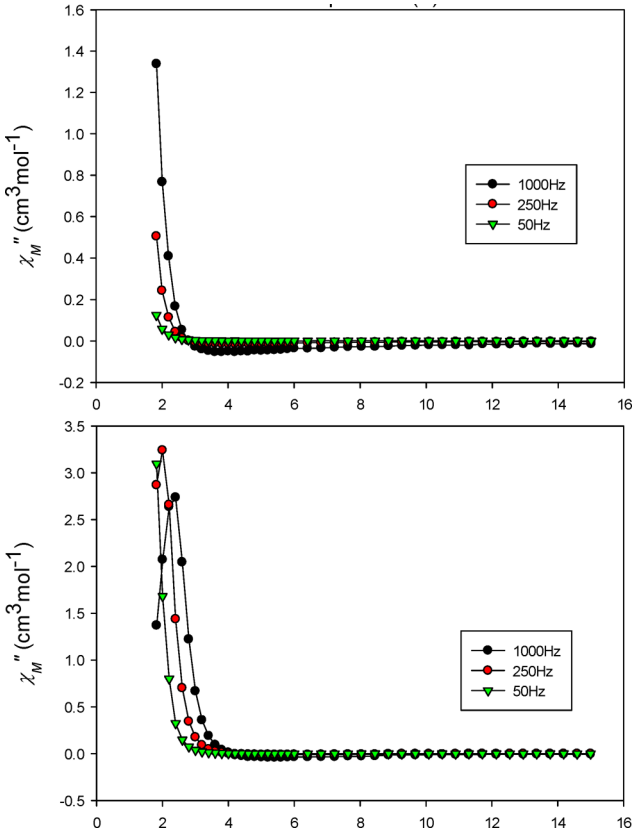

Figure 11. Out-of-phase ac χ''_M vs T at the indicated frequencies for (top) **1**·2H_2O and (bottom) **2**·H_2O. The solid lines are guides for the eye.

∼4 cm^3 K mol^{-1}, respectively, consistent with S = 4, and $^5/_2$ ground states with g < 2 (Figure 12). No (or essentially no) χ''_M signals were observed down to 1.8 K for **3**·2H_2O, **4**, or **5** (Figure S8).

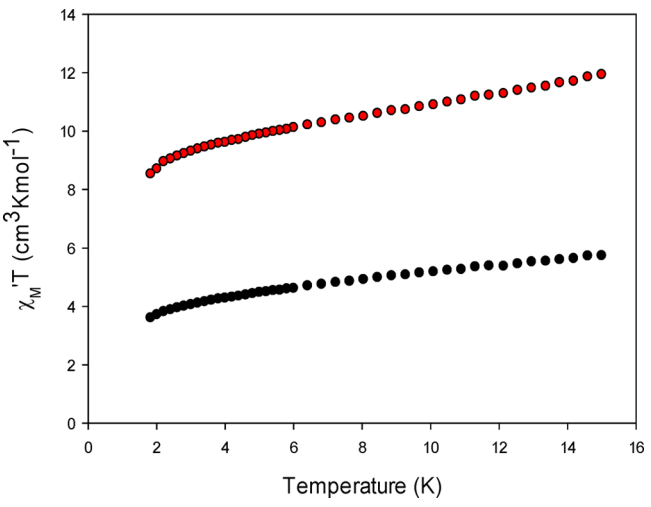

Figure 12. In-phase ac χ'_MT vs T at the indicated frequencies for **3**·2H_2O (red ●) and **4** (black ●).

CONCLUSIONS

Complete substitution with $Ph_2PO_2^-$ of all carboxylates in $[Mn_3O(O_2CMe)_3(mpko)_3]^+$ has been accomplished with essentially no structural change to the cluster. On the basis of the similar elemental analysis and magnetic data, the same is also true for the bulkier $ppko^-$ analogue. Small changes to Mn···Mn separations and Mn−N−O−Mn torsion angles do occur, and there is some reason to believe the structure is more equilateral than the carboxylate analogues. Such small changes notwithstanding, the properties of the carboxylate versus phosphinate clusters are very similar, both types being **F** with S = 6 ground states, and consequently the new phosphinate clusters are also new members of the family of Mn-containing SMMs. We suspect the $mpko^-$ and $ppko^-$ ancillary ligands help to prevent any structural/nuclearity change on carboxylate substitution by stabilizing the triangular Mn_3 structure through their chelating/bridging binding modes. In contrast, $PhPO_3^{2-}$ appears to cause rupture of the Mn_3 structure, giving an insoluble (likely polymeric) product that unfortunately we were not able to characterize. However, an interesting and soluble Mn_9 cluster with $PhPO_3^{2-}$ was obtained from a reaction with simple Mn reagents. Finally, **5** contains no carboxylates or phosphonates, and its triangular structure with three $mpko^-$ groups supports the belief stated above about the importance of these groups in the robustness of the Mn_3 triangle during carboxylate substitution. One general conclusion from this work is that carboxylate substitution with $Ph_2PO_2^-$, notwithstanding its greater bulk, may be of greater utility as a means of modifying the ligation environment of SMMs without structural change than previously thought, even for clusters with moderate levels of carboxylate content.

ASSOCIATED CONTENT

Supporting Information

The Supporting Information is available free of charge on the ACS Publications website at DOI: 10.1021/acs.inorgchem.7b01793.

Tables of selected bond distances and angles for **1**·5CH_2Cl_2, **3**·2MeOH, **4**·10MeCN, and **5**; structural figures; bond valence sums; magnetic data (reduced magnetization plots and error surfaces) for **3**·2H_2O, **4**, and **5** (PDF)

Accession Codes

CCDC 1561625−1561628 contain the supplementary crystallographic data for this paper. These data can be obtained free of charge via www.ccdc.cam.ac.uk/data_request/cif, or by emailing data_request@ccdc.cam.ac.uk, or by contacting The Cambridge Crystallographic Data Centre, 12 Union Road, Cambridge CB2 1EZ, UK; fax: +44 1223 336033.

AUTHOR INFORMATION

Corresponding Author

*E-mail: christou@chem.ufl.edu. Phone: +1-352-392-8314. Fax: +1-352-392-8757.

ORCID

George Christou: 0000-0001-5923-5523

Present Address

†Intel Corporation, Hillsboro, OR.

Notes

The authors declare no competing financial interest.

DOI: 10.1021/acs.inorgchem.7b01793
Inorg. Chem. 2017, 56, 11352−11364

■ ACKNOWLEDGMENTS

We thank the National Science Foundation (Grant No. CHE-1565664) for support of this work.

■ REFERENCES

(1) (a) Sessoli, R.; Gatteschi, D.; Caneschi, A.; Novak, M. Magnetic bistability in a metal-ion cluster. *Nature* **1993**, *365*, 141−143. (b) Sessoli, R.; Tsai, H.; Schake, A.; Wang, S.; Vincent, J.; Folting, K.; Gatteschi, D.; Christou, G.; Hendrickson, D. High-spin molecules: [Mn12O12(O2CR)16(H2O)4]. *J. Am. Chem. Soc.* **1993**, *115*, 1804−1816.

(2) (a) Christou, G.; Gatteschi, D.; Hendrickson, D.; Sessoli, R. Single-Molecule Magnets. *MRS Bull.* **2000**, *25*, 66−71. (b) Hendrickson, D. N.; Christou, G.; Ishimoto, H.; Yoo, J.; Brechin, E. K.; Yamaguchi, A.; Rumberger, E. M.; Aubin, S. M. J.; Sun, Z. M.; Aromi, G. Magnetization tunneling in single-molecule magnets. *Polyhedron* **2001**, *20*, 1479−1488.

(3) Aromi, G.; Brechin, E. K. Synthesis of 3d metallic single-molecule magnets. *Struct. Bonding (Berlin)* **2006**, *122*, 1−67.

(4) Bagai, R.; Christou, G. The Drosophila of single-molecule magnetism: $[Mn_{12}O_{12}(O_2CR)_{16}(H_2O)_4]$. *Chem. Soc. Rev.* **2009**, *38*, 1011−1026.

(5) Craig, G. A.; Murrie, M. 3d single-ion magnets. *Chem. Soc. Rev.* **2015**, *44*, 2135−2147.

(6) (a) Rinehart, J. D.; Fang, M.; Evans, W. J.; Long, J. R. Strong exchange and magnetic blocking in N_2^{3-}-radical-bridged lanthanide complexes. *Nat. Chem.* **2011**, *3*, 538−542. (b) Rinehart, J. D.; Fang, M.; Evans, W. J.; Long, J. R. A N2(3-) radical-bridged terbium complex exhibiting magnetic hysteresis at 14 K. *J. Am. Chem. Soc.* **2011**, *133*, 14236−14239.

(7) (a) Woodruff, D. N.; Winpenny, R. E.; Layfield, R. A. Lanthanide single-molecule magnets. *Chem. Rev.* **2013**, *113*, 5110−5148. (b) Liddle, S. T.; van Slageren, J. Improving f-element single molecule magnets. *Chem. Soc. Rev.* **2015**, *44*, 6655−6669.

(8) (a) Pereira, L. C. J.; Camp, C.; Coutinho, J. T.; Chatelain, L.; Maldivi, P.; Almeida, M.; Mazzanti, M. Single-Molecule-Magnet Behavior in Mononuclear Homoleptic Tetrahedral Uranium(III) Complexes. *Inorg. Chem.* **2014**, *53*, 11809−11811. (b) Moro, F.; Mills, D. P.; Liddle, S. T.; van Slageren, J. The Inherent Single-Molecule Magnet Character of Trivalent Uranium. *Angew. Chem., Int. Ed.* **2013**, *52*, 3430−3433.

(9) (a) Osa, S.; Kido, T.; Matsumoto, N.; Re, N.; Pochaba, A.; Mrozinski, J. A Tetranuclear 3d−4f Single Molecule Magnet: $[Cu^{II}LTb^{III}(hfac)_2]_2$. *J. Am. Chem. Soc.* **2004**, *126*, 420−421. (b) Zaleski, C. M.; Depperman, E. C.; Kampf, J. W.; Kirk, M.-L.; Pecoraro, V. L. Synthesis, Structure, and Magnetic Properties of a Large Lanthanide−Transition-Metal Single-Molecule Magnet. *Angew. Chem., Int. Ed.* **2004**, *43*, 3912−3914. (c) Mishra, A.; Wernsdorfer, W.; Abboud, K. A.; Christou, G. Initial Observation of Magnetization Hysteresis and Quantum Tunneling in Mixed Manganese−Lanthanide Single-Molecule Magnets. *J. Am. Chem. Soc.* **2004**, *126*, 15648−15649.

(10) (a) Mereacre, V.; Ako, A. M.; Clerac, R.; Wernsdorfer, W.; Hewitt, I. J.; Anson, C. E.; Powell, A. K. Heterometallic $[Mn_5\text{-}Ln_4]$ Single-Molecule Magnets with High Anisotropy Barriers. *Chem. - Eur. J.* **2008**, *14*, 3577−3584. (c) Langley, S.; Moubaraki, B.; Murray, K. S. A heptadecanuclear $Mn^{III}_9Dy^{III}_8$ cluster derived from triethanolamine with two edge sharing supertetrahedra as the core and displaying SMM behavior. *Dalton Trans.* **2010**, *39*, 5066−5069. (d) Karotsis, G.; Kennedy, S.; Teat, S. J.; Beavers, C. M.; Fowler, D. A.; Morales, J. J.; Evangelisti, M.; Dalgarno, S. J.; Brechin, E. K. $[Mn^{III}_4Ln^{III}_4]$ Calix[4]arene Clusters as Enhanced Magnetic Coolers and Molecular Magnets. *J. Am. Chem. Soc.* **2010**, *132*, 12983−12990. (e) Sessoli, R.; Powell, A. K. Strategies towards single molecule magnets based on lanthanide ions. *Coord. Chem. Rev.* **2009**, *253*, 2328−2341. (f) Liu, C.-M.; Zhang, D.-Q.; Zhu, D.-B. Heptanuclear 3d−4f cluster complexes with a coaxial double-screw-propeller topology and diverse magnetic properties. *Dalton Trans.* **2010**, *39*, 11325−11328.

(11) Rosado Piquer, L.; Sanudo, E. C. Heterometallic 3d−4f single-molecule magnets. *Dalton Trans.* **2015**, *44*, 8771−8780.

(12) Guo, F.-S.; Layfield, R. A.; Day, B.; Chen, Y.-C.; Tong, M.-L.; Mansikkamäki, A. A dysprosium metallocene single-molecule magnet functioning at the axial limit. *Angew. Chem., Int. Ed.* **2017**, *56*, 1−6.

(13) (a) Friedman, J.; Sarachik, M.; Tejada, J.; Ziolo, R. Macroscopic Measurement of Resonant Magnetization Tunneling in High-Spin Molecules. *Phys. Rev. Lett.* **1996**, *76*, 3830−3833. (b) Thomas, L.; Lionti, F.; Ballou, R.; Gatteschi, D.; Sessoli, R.; Barbara, B. Macroscopic quantum tunnelling of magnetization in a single crystal of nanomagnets. *Nature* **1996**, *383*, 145−147. (c) Friedman, J.; Sarachik, M.; Tejada, J.; Maciejewski, J.; Ziolo, R. Steps in the hysteresis loops of a high-spin molecule. *J. Appl. Phys.* **1996**, *79*, 6031−6033.

(14) (a) Wernsdorfer, W.; Sessoli, R. Quantum phase interference and parity effects in magnetic molecular clusters. *Science* **1999**, *284*, 133−135. (b) Wernsdorfer, W.; Soler, M.; Christou, G.; Hendrickson, D. N. *Quantum phase interference (Berry phase) in single-molecule magnets of* $[Mn_{12}]^{2-}$. (c) Lecren, L.; Wernsdorfer, W.; Li, Y. G.; Roubeau, O.; Miyasaka, H.; Clerac, R. Quantum Tunneling and Quantum Phase Interference in a $[Mn^{II}_2Mn^{III}_2]$ Single-Molecule Magnet. *J. Am. Chem. Soc.* **2005**, *127*, 11311−11317. (d) Wernsdorfer, W.; Chakov, N. E.; Christou, G. Quantum Phase Interference and Spin-Parity in Mn12 Single-Molecule Magnets. *Phys. Rev. Lett.* **2005**, *95*.10.1103/PhysRevLett.95.037203

(15) (a) Wernsdorfer, W.; Aliaga-Alcalde, N.; Hendrickson, D. N.; Christou, G. Exchange-biased quantum tunnelling in a supramolecular dimer of single-molecule magnets. *Nature* **2002**, *416*, 406−409. (b) Yang, E. C.; Wernsdorfer, W.; Hill, S.; Edwards, R. S.; Nakano, M.; Maccagnano, S.; Zakharov, L. N.; Rheingold, A. L.; Christou, G.; Hendrickson, D. N. Exchange bias in Ni_4 single-molecule magnets. *Polyhedron* **2003**, *22*, 1727−1733.

(16) (a) Pinkowicz, D.; Southerland, H. I.; Avendaño, C.; Prosvirin, A.; Sanders, C.; Wernsdorfer, W.; Pedersen, K. S.; Dreiser, J.; Clérac, R.; Nehrkorn, J.; Simeoni, G. G.; Schnegg, A.; Holldack, K.; Dunbar, K. R. Cyanide Single-Molecule Magnets Exhibiting Solvent Dependent Reversible "On" and "Off" Exchange Bias Behavior. *J. Am. Chem. Soc.* **2015**, *137*, 14406−14422. (b) Nguyen, T. N.; Wernsdorfer, W.; Shiddiq, M.; Abboud, K. A.; Hill, S.; Christou, G. Supramolecular Aggregates of Single-Molecule Magnets: Exchange-biased Quantum Tunneling of Magnetization in a Rectangular $[Mn_3]_4$ Tetramer. *Chem. Sci.* **2016**, *7*, 1156−1173.

(17) (a) Affronte, M.; Troiani, F.; Ghirri, A.; Candini, A.; Evangelisti, M.; Corradini, V.; Carretta, S.; Santini, P.; Amoretti, G.; Tuna, F.; Timco, G.; Winpenny, R. E. P. Single molecule magnets for quantum computation. *J. Phys. D: Appl. Phys.* **2007**, *40*, 2999−3004. (b) Affronte, M. Molecular nanomagnets for information technologies. *J. Mater. Chem.* **2009**, *19*, 1731−1737. (c) Leuenberger, M. N.; Loss, D. Quantum computing in molecular magnets. *Nature* **2001**, *410*, 789.

(18) (a) Bogani, L.; Wernsdorfer, W. Molecular spintronics using single-molecule magnets. *Nat. Mater.* **2008**, *7*, 179−186. (b) Urdampilleta, M.; Klyatskaya, S.; Cleuziou, J.-P.; Ruben, M.; Wernsdorfer, W. Supramolecular spin valves. *Nat. Mater.* **2011**, *10*, 502−506.

(19) Mukherjee, S.; Abboud, K. A.; Wernsdorfer, W.; Christou, G. Comproportionation Reactions to Manganese(III/IV) Pivalate Clusters: A New Half-Integer Spin Single-Molecule Magnet. *Inorg. Chem.* **2013**, *52*, 873−884.

(20) (a) King, P.; Wernsdorfer, W.; Abboud, K. A.; Christou, G. A Family of Mn_{16} Single-Molecule Magnets from a Reductive Aggregation Route. *Inorg. Chem.* **2004**, *43*, 7315−7323. (b) Tasiopoulos, A. J.; Wernsdorfer, W.; Abboud, K. A.; Christou, G. Two isomeric $[Mn_{12}O_{12}(OMe)_2(O_2CPh)_{16}(H_2O)_2]^{2-}$ single-molecule magnets and a Mn^{III} polymer prepared by a reductive aggregation synthetic route. *Polyhedron* **2005**, *24*, 2505−2512. (c) Thuijs, A. L. E.; King, P.; Abboud, K. A.; Christou, G. New Structural Types of Mn_{16} Single-Molecule Magnets: W-Shaped Topology from Reductive Aggregation. *Inorg. Chem.* **2015**, *54*, 9127−9137.

(21) Vinslava, A.; Tasiopoulos, A. J.; Wernsdorfer, W.; Abboud, K. A.; Christou, G. Molecules at the Quantum−Classical Nanoparticle

DOI: 10.1021/acs.inorgchem.7b01793
Inorg. Chem. 2017, 56, 11352−11364

Interface: Giant Mn_{70} Single-Molecule Magnets of ~ 4 nm Diameter. *Inorg. Chem.* **2016**, *55*, 3419−3430.
(22) Moro, F.; Biagi, R.; Corradini, V.; Evangelisti, M.; Gambardella, A.; De Renzi, V.; del Pennino, U.; Coronado, E.; Forment-Aliaga, A.; Romero, F. M. Electronic and Magnetic Properties of Mn_{12} Molecular Magnets on Sulfonate and Carboxylic Acid Prefunctionalized Gold Surfaces. *J. Phys. Chem. C* **2012**, *116*, 14936−14942.
(23) Inglis, R.; Dalgarno, S. J.; Brechin, E. K. A new family of Mn_6 SMMs using phosphinate ligands. *Dalton Trans* **2010**, *39*, 4826−4831.
(24) Lis, T. Preparation, Structure, and Magnetic Properties of a Dodeeanuelear Mixed-Valence Manganese Carboxylate. *Acta Crystallogr., Sect. B: Struct. Crystallogr. Cryst. Chem.* **1980**, *36*, 2042−2046.
(25) Brockman, J. T.; Abboud, K. A.; Hendrickson, D. N.; Christou, G. A new family of Mn_{12} single-molecule magnets: replacement of carboxylate ligands with diphenylphosphinates. *Polyhedron* **2003**, *22*, 1765−1769.
(26) (a) Bian, G.-Q.; Kuroda-Sowa, T.; Konaka, H.; Hatano, M.; Maekawa, M.; Munakata, M.; Miyasaka, H.; Yamashita, M. A Mn_{12} Single-Molecule Magnet $[Mn_{12}O_{12}(OAc)_{12}(dpp)_4]$ (dppH = diphenyl phosphate) with no coordinating water Molecules. *Inorg. Chem.* **2004**, *43*, 4790−4792.
(27) Chakov, N. E.; Abboud, K. A.; Zakharov, L. N.; Rheingold, A. L.; Hendrickson, D. N.; Christou, G. Reaction of $[Mn_{12}O_{12}(O_2CR)_{16}(H_2O)_4]$ single-molecule magnets with non-carboxylate ligands. *Polyhedron* **2003**, *22*, 1759−1763.
(28) Chakov, N. E.; Wernsdorfer, W.; Abboud, K. A.; Christou, G. Mixed-Valence $Mn^{III}Mn^{IV}$ Clusters $[Mn_7O_8(O_2SePh)_8(O_2CMe)(H_2O)]$ and $[Mn_7O_8(O_2SePh)_9(H_2O)]$: Single-Chain Magnets Exhibiting Quantum Tunneling of Magnetization. *Inorg. Chem.* **2004**, *43*, 5919−5930.
(29) Chakov, N. E.; Thuijs, A. E.; Wernsdorfer, W.; Rheingold, A. L.; Abboud, K. A.; Christou, G. Unusual $Mn^{III/IV}_4$ Cubane and $Mn^{III}_{16}M_4$ (M = Ca, Sr) Looplike Clusters from the Use of Dimethylarsinic Acid. *Inorg. Chem.* **2016**, *55*, 8468−8477.
(30) Nguyen, T. N.; Shiddiq, M.; Ghosh, T.; Abboud, K. A.; Hill, S.; Christou, G. Covalently linked dimer of Mn_3 single-molecule magnets and retention of its structure and quantum properties in solution. *J. Am. Chem. Soc.* **2015**, *137*, 7160−7168.
(31) Stamatatos, T. C.; Foguet-Albiol, D.; Lee, S. C.; Stoumpos, C. C.; Raptopoulou, C. P.; Terzis, A.; Wernsdorfer, W.; Hill, S. O.; Perlepes, S. P.; Christou, G. Switching On" the Properties of Single-Molecule Magnetism in Triangular Manganese(III) Complexes. *J. Am. Chem. Soc.* **2007**, *129*, 9484−99.
(32) (a) Sala, T.; Sargent, M. V. Tetrabutylammonium permanganate: an efficient oxidant for organic substrates. *J. Chem. Soc., Chem. Commun.* **1978**, 253−254. (b) Vincent, J. B.; Folting, K.; Huffman, J. C.; Christou, G. Use of tetra-n-butylammonium permanganate for inorganic syntheses in nonaqueous solvents. Preparation and structure of a manganese(III) dimer containing bridging phenoxo oxygen atoms. *Inorg. Chem.* **1986**, *25*, 996−999.
(33) Orama, M.; Saarinen, H.; Korvenranta, J. Formation of trinuclear copper(II) complexes with three pyridine oxime ligands in aqueous solution. *J. Coord. Chem.* **1990**, *22*, 183−190.
(34) Milios, C. J.; Stamatatos, T. C.; Kyritsis, P.; Terzis, A.; Raptopoulou, C. P.; Vicente, R.; Escuer, A.; Perlepes, S. P. Phenyl 2-Pyridyl Ketone and Its Oxime in Manganese Carboxylate Chemistry: Synthesis, Characterisation, X-ray Studies and Magnetic Properties of Mononuclear, Trinuclear and Octanuclear Complexes. *Eur. J. Inorg. Chem.* **2004**, *2004*, 2885−2901.
(35) Vincent, J. B.; Chang, H. R.; Folting, K.; Huffman, J. C.; Christou, G.; Hendrickson, D. N. Preparation and physical properties of trinuclear oxo-centered manganese complexes of the general formulation $[Mn_3O(O_2CR)_6L_3]^+$ (R = Me or Ph; L = a neutral donor group) and the crystal structures of $[Mn_3O(O_2CPh)_6(pyr)_2(H_2O)]\cdot 0.5MeCN$. *J. Am. Chem. Soc.* **1987**, *109*, 5703−5711.
(36) Bruker. *SAINT,* 6.36a; Bruker AXS, Inc: Madison, WI, 1998.
(37) (a) Vandersluis, P.; Spek, A. L. BYPASS: an effective method for the refinement of crystal structures containing disordered solvent regions. *Acta Crystallogr., Sect. A: Found. Crystallogr.* **1990**, *46*, 194−201. (b) Spek, A. L. PLATON SQUEEZE: a tool for the calculation of the disordered solvent contribution to the calculated structure factors. *Acta Crystallogr., Sect. C: Struct. Chem.* **2015**, *71*, 9−18.
(38) Spek, A. L. Structure validation in chemical crystallography. *Acta Crystallogr., Sect. D: Biol. Crystallogr.* **2009**, *65*, 148−155.
(39) Davidson, E. R. *MAGNET;* Indiana University: Bloomington, IN, 1999.
(40) West, R. C. *CRC Handbook of Chemistry and Physics;* CRC Press Inc.: Boca Raton, FL, 1984.
(41) Eppley, H. J.; Tsai, H. L.; Devries, N.; Folting, K.; Christou, G.; Hendrickson, D. N. High-Spin Molecules: Unusual Magnetic Susceptibility Relaxation Effects in $[Mn_{12}O_{12}(O_2CEt)_{16}(H_2O)_3]$ (S = 9) and the One-Electron Reduction Product $(PPh_4)[Mn_{12}O_{12}(O_2CEt)_{16}(H_2O)_4]$ ($S = {}^{19}/_2$). *J. Am. Chem. Soc.* **1995**, *117*, 301−317.
(42) Van Vleck, J. H. *The Theory of Electric and Magnetic Susceptibilities;* Oxford University Press: London, England, 1965.
(43) Cannon, R. D.; Jayasooriya, U. A.; Wu, R. W.; Arapkoske, S. K.; Stride, J. A.; Nielsen, O. F.; White, R. P.; Kearley, G. J.; Summerfield, D. Spin frustration in high-spin triiron(III) complexes: an inelastic neutron scattering study. *J. Am. Chem. Soc.* **1994**, *116*, 11869−11874.
(44) (a) Milios, C. J.; Piligkos, S.; Brechin, E. K. Ground state spin-switching via targeted structural distortion: twisted single-molecule magnets from derivatised salicylaldoximes. *Dalton Trans* **2008**, 1809−1817. (b) Milios, C. J.; Vinslava, A.; Wernsdorfer, W.; Prescimone, A.; Wood, P. A.; Parsons, S.; Perlepes, S. P.; Christou, G.; Brechin, E. K. Spin Switching via Targeted Structural Distortion. *J. Am. Chem. Soc.* **2007**, *129*, 6547−6561. (c) Martinez-Lillo, J.; Tomsa, A. R.; Li, Y. L.; Chamoreau, L. M.; Cremades, E.; Ruiz, E.; Barra, A. L.; Proust, A.; Verdaguer, M.; Gouzerh, P. Synthesis, crystal structure and magnetism of new salicylamidoxime-based hexanuclear manganese(III) single-molecule magnets. *Dalton Trans* **2012**, *41*, 13668−13681. (d) Inglis, R.; Jones, L. F.; Milios, C. J.; Datta, S.; Collins, A.; Parsons, S.; Wernsdorfer, W.; Hill, S.; Perlepes, S. P.; Piligkos, S.; Brechin, E. K. Attempting to understand (and control) the relationship between structure and magnetism in an extended family of Mn_6 single-molecule magnets. *Dalton Trans* **2009**, 3403−3412.
(45) Davidson, E. R. *GRID;* Indiana University: Bloomington, IN, 1999.
(46) (a) Bao, S.-S.; Zheng, L.-M. Magnetic materials based on 3d metal phosphonates. *Coord. Chem. Rev.* **2016**, *319*, 63−85. (b) Sheikh, J. A.; Jena, H. S.; Clearfield, A.; Konar, S. Phosphonate Based High Nuclearity Magnetic Cages. *Acc. Chem. Res.* **2016**, *49*, 1093−1103.
(47) (a) Shanmugam, M.; Chastanet, G.; Mallah, T.; Sessoli, R.; Teat, S. J.; Timco, G. A.; Winpenny, R. E. P. Synthesis and Characterization of Mixed-Valent Manganese Phosphonate Cage Complexes. *Chem. - Eur. J.* **2006**, *12*, 8777−8785. (b) Wang, M.; Ma, C.; Chen, C. Synthesis and characterization of nona- and trideca-nuclear manganese phosphonate clusters. *Dalton Trans* **2008**, 4612−4620.
(48) (a) Kessissoglou, D. P.; Kirk, M. L.; Lah, M. S.; Li, X. H.; Raptopoulou, C.; Hatfield, W. E.; Pecoraro, V. L. Structural and magnetic characterization of trinuclear, mixed-valence manganese acetates. *Inorg. Chem.* **1992**, *31*, 5424−5432. (b) Tangoulis, V.; Malamatari, D. A.; Soulti, K.; Stergiou, V.; Raptopoulou, C. P.; Terzis, A.; Kabanos, T. A.; Kessissoglou, D. P. Manganese(II/II/II) and Manganese(III/II/III) trinuclear compounds. structure and solid and solution behavior. *Inorg. Chem.* **1996**, *35*, 4974−4983. (c) Pal, S.; Chan, M. K.; Armstrong, W. H. Ground spin state variability in manganese oxo aggregates. Demonstration of an S = 3/2 ground state for $[Mn_3O_4(OH)(bpea)_3](ClO_4)_3$. *J. Am. Chem. Soc.* **1992**, *114*, 6398−6406. (d) Ribas, J.; Albela, B.; StoeckliEvans, H.; Christou, G. Synthesis and magnetic properties of six new trinuclear oxo-centered manganese complexes of general formula $[Mn_3O(X\text{-benzoato})_6L_3]$ (X = 2-F, 2-Cl, 2-Br, 3-F, 3-Cl, 3-Br; L = pyridine or water) and crystal structures of the 2-F, 3-Cl, and 3-Br complexes. *Inorg. Chem.* **1997**, *36*, 2352−2360.
(49) Inglis, R.; Taylor, S. M.; Jones, L. F.; Papaefstathiou, G. S.; Perlepes, S. P.; Datta, S.; Hill, S.; Wernsdorfer, W.; Brechin, E. K.

DOI: 10.1021/acs.inorgchem.7b01793
Inorg. Chem. 2017, 56, 11352−11364

Twisting, bending, stretching: strategies for making ferromagnetic $[Mn^{III}_3]$ triangles. *Dalton Trans* **2009**, 9157−9168.

DOI: 10.1021/acs.inorgchem.7b01793
Inorg. Chem. 2017, 56, 11352−11364